Weakly nonlinear analysis of impulsively-forced Faraday waves

Anne Catllá,[1,*] Jeff Porter,[2] and Mary Silber[1]

[1]*Department of Engineering Sciences and Applied Mathematics, Northwestern University, Evanston, Illinois 60208, USA*

[2]*Instituto Pluridisciplinar, Universidad Complutense de Madrid, 28040 Madrid, Spain*

(Received 11 January 2005; published 17 November 2005)

Parametrically-excited surface waves, forced by a repeating sequence of N delta-function impulses, are considered within the framework of the Zhang-Viñals model [W. Zhang and J. Viñals, J. Fluid Mech. **336**, 301 (1997)]. With impulsive forcing, the linear stability analysis can be carried out exactly and leads to an implicit equation for the neutral stability curves. As noted previously [J. Bechhoefer and B. Johnson, Am. J. Phys. **64**, 1482 (1996)], in the simplest case of $N=2$ *equally-spaced* impulses per period (which alternate up and down) there are only subharmonic modes of instability. The familiar situation of alternating subharmonic and harmonic resonance tongues emerges only if an asymmetry in the spacing between the impulses is introduced. We extend the linear analysis for $N=2$ impulses per period to the weakly nonlinear regime, where we determine the leading order nonlinear saturation of one-dimensional standing waves as a function of forcing strength. Specifically, an analytic expression for the cubic Landau coefficient in the bifurcation equation is derived as a function of the dimensionless spacing between the two impulses and the fluid parameters that appear in the Zhang-Viñals model. As the capillary parameter is varied, one finds a parameter regime of wave amplitude suppression, which is due to a familiar 1:2 spatiotemporal resonance between the subharmonic mode of instability and a damped harmonic mode. This resonance occurs for impulsive forcing even when harmonic resonance tongues are absent from the neutral stability curves. The strength of this resonance feature can be tuned by varying the spacing between the impulses. This finding is interpreted in terms of a recent symmetry-based analysis of multifrequency forced Faraday waves [J. Porter, C. M. Topaz, and M. Silber, Phys. Lett. **93**, 034502 (2004); C. M. Topaz, J. Porter, and M. Silber, Phys. Rev. E **70**, 066206 (2004)].

DOI: 10.1103/PhysRevE.72.056212 PACS number(s): 05.45.−a, 47.35.+i, 47.54.+r, 89.75.Kd

I. INTRODUCTION

Standing waves form spontaneously on the free surface of a fluid layer when it is subjected to a time-periodic vertical vibration of sufficient strength. The waves, which result from a symmetry-breaking parametric instability, organize themselves into remarkably regular patterns, as first described by Faraday in 1831 [1]. In modern experiments, various container geometries, fluids, and forcing functions have been employed, resulting in a rich variety of standing wave patterns, as well as a range of dynamical responses. See [2,3] for reviews on Faraday waves. In this paper, we investigate the response of the Faraday system to an idealized forcing function consisting of a periodic sequence of delta-function impulses. The results are contrasted with those obtained in the classical cases of single and multifrequency forcing.

The versatility of the Faraday system for investigating pattern formation owes much to the vastness of its control parameter space. By varying the forcing frequency and amplitude of a sinusoidal acceleration function, as well as the fluid properties, experimentalists have teased out spatially regular patterns ranging from stripes, hexagons and squares to targets, spirals and quasipatterns [4–7]. The seminal experiments of Edwards and Fauve [8] showed how the addition of a second commensurate frequency component in the forcing function could lead to even greater versatility of this system, via the controlled introduction of additional length scales. Two-frequency forcing has led to various exotic superlattice patterns [9,10], as well as quasipatterns [11,12], triangular patterns [13], and localized structures [14]. A detailed description of patterns readily achieved in two-frequency Faraday experiments can be found in [15]. Recent experiments by Epstein and Fineberg [16] have employed a third perturbing frequency to rapidly switch between the novel patterns achieved with two-frequency forcing.

Theoretically, the Faraday system presents a number of challenges due both to the explicit time dependence of the forcing and the free-boundary nature of the problem; for a partial review of theoretical work see [3]. Consequently, models incorporating simplifying assumptions have often been relied on, in conjunction with numerical linear stability analysis or perturbative methods. Linear stability results build on the classic paper of Benjamin and Ursell [17], who showed that the linear stability problem, in the case of an ideal fluid, reduces to a Mathieu equation, thereby explaining Faraday's observation of a subharmonic response of the fluid layer to sinusoidal forcing. Subsequent investigators carried out linear stability analyses for a viscous fluid layer subjected to sinusoidal forcing [18–21]. These results were also extended to two-frequency forcing in [22]. Theoretical understanding of the nonlinear problem progressed with the introduction of a quasipotential formulation of the Faraday wave problem by Zhang and Viñals [23]. This model, which describes small amplitude surface waves on a semi-infinite,

*Electronic address: acatlla@math.duke.edu

weakly viscous fluid layer, eliminates the bulk flow, assumed to be potential, from the description. The free boundary $z=h(\mathbf{x},t)$ $(\mathbf{x}\in\mathbb{R}^2)$ is then prescribed by an evolution equation for h, which is coupled to an evolution equation for a surface velocity potential Φ; see Sec. II. Zhang and Viñals used this model to further investigate nonlinear effects via an asymptotic expansion, which demonstrated the importance of resonant triads (three-wave resonance) in the pattern selection process.

The investigations reviewed above focus on Faraday waves parametrically excited by sinusoidal and multifrequency forcing functions. An alternative forcing function, consisting of a periodic sequence of delta-function impulses, was proposed by Bechhoefer and Johnson [24] who indicated how the linear analysis could be greatly simplified in this case. (This idealization of parametrically forced systems has been put forth in a variety of physical contexts; see, for example, [25–27].) Recently, Huepe and Silber [28] showed that the linear analysis of the impulsively-forced Faraday problem for a viscous fluid, as proposed in [24], breaks down in certain parameter regimes. In these regimes, the flow in the fluid bulk cannot be (instantaneously) matched across the delta impulses. However, these complications are absent from the Zhang-Viñals formulation, which describes the evolution of the free surface, with the bulk flow eliminated from the model. In this paper we extend the results of Bechhoefer and Johnson on impulsively-forced Faraday waves into the weakly nonlinear regime, within the framework of the Zhang-Viñals model.

Following the method of [25], we develop a simple modular approach to constructing the stroboscopic map associated with the linear stability problem. Specifically, we construct the linear maps which evolve perturbations of wave number k from one impulse in the sequence to the next. From this simple construction we can derive explicit expressions for the Floquet multipliers associated with the linear stability problem, and arrive at an equation (implicit if $N>2$) that describes the neutral stability curves.

We extend the analysis for $N=2$ impulses per period to the weakly nonlinear regime for one-dimensional surface waves. A key observation of Bechhoefer and Johnson [24] is that there are no harmonic resonance tongues for a sequence of $N=2$ impulses if they are equally spaced in time (i.e., an up impulse and then a down impulse half a period later). We show that, despite the absence of harmonic instabilities, there can still be a significant resonant interaction between the excited subharmonic and damped harmonic modes which leads, in one dimension, to an associated degradation in the (weakly) nonlinear response of the fluid to the vibration. This is similar to the spatiotemporal 1:2 resonance that occurs in the case of sinusoidal forcing [23]. In addition to analyzing the case of $N=2$ *equally-spaced* impulses, we explore the effects of varying the spacing between the impulses so that they are no longer exactly half a period apart. We find that this asymmetry in impulse timing enhances or diminishes the influence of the 1:2 resonance on the standing wave amplitude depending on the sense in which it is applied. We understand this result by considering a two-term Fourier series approximation to the impulsive forcing function, and applying recent results pertaining to multifrequency forcing [29,30].

Our paper is organized as follows. In the next section we present the Zhang-Viñals model of Faraday waves and carry out the linear stability analysis in the general case of N impulses per forcing period. We then focus on the simplest case of $N=2$ and compare our results with those obtained for sinusoidal and multifrequency forcing functions. In Sec. III we derive the cubic bifurcation equation that determines the amplitude of one-dimensional spatially-periodic surface waves driven by impulsive forcing, focusing on the 1:2 spatiotemporal resonance feature. We compare our weakly nonlinear results with those obtained for single and two-frequency forced Faraday waves. Finally, in Sec. IV, we summarize our results and indicate some directions for subsequent investigations.

II. LINEAR RESULTS FOR THE ZHANG-VIÑALS FARADAY WAVE MODEL

A. Zhang-Viñals model

The quasipotential formulation of the Faraday wave problem, due to Zhang and Viñals [23], is derived from the Navier-Stokes equations assuming small amplitude surface waves on a deep, nearly inviscid fluid layer. It describes the free surface height $h(\mathbf{x},t)$ and surface velocity potential $\Phi(\mathbf{x},t)$ of a fluid subjected to a (dimensionless) periodic vertical acceleration function $G(t)$. Employing these equations greatly simplifies our calculations since the flow in the bulk does not appear explicitly—we need only to track the behavior of the free surface, a function of the horizontal coordinate $\mathbf{x}\in\mathbb{R}^2$ and time t. The Zhang-Viñals model takes the form

$$(\partial_t-\gamma\nabla^2)h-\hat{D}\Phi=N_1(h,\Phi), \tag{1a}$$

$$(\partial_t-\gamma\nabla^2)\Phi-[\Gamma_0\nabla^2-G_0+G(t)]h=N_2(h,\Phi), \tag{1b}$$

where the nonlinear terms in (1) are given by

$$\begin{aligned}N_1(h,\Phi)=&-\boldsymbol{\nabla}\cdot(h\,\boldsymbol{\nabla}\,\Phi)+\frac{1}{2}\nabla^2(h^2\hat{D}\Phi)-\hat{D}(h\hat{D}\Phi)\\&+\hat{D}\left[h\hat{D}(h\hat{D}\Phi)+\frac{1}{2}h^2\nabla^2\Phi\right],\end{aligned} \tag{2a}$$

$$\begin{aligned}N_2(h,\Phi)=&\frac{1}{2}(\hat{D}\Phi)^2-\frac{1}{2}(\boldsymbol{\nabla}\Phi)^2-\frac{1}{2}\Gamma_0\,\boldsymbol{\nabla}\cdot[(\boldsymbol{\nabla}h)(\boldsymbol{\nabla}h)^2]\\&-(\hat{D}\Phi)[h\nabla^2\Phi+\hat{D}(h\hat{D}\Phi)].\end{aligned} \tag{2b}$$

Here the operator $\hat{D}$ multiplies each Fourier component by its wave number, e.g., $\hat{D}e^{i\mathbf{k}\cdot\mathbf{x}}=|\mathbf{k}|e^{i\mathbf{k}\cdot\mathbf{x}}$, and the dimensionless fluid parameters are

$$\gamma\equiv\frac{2\nu k_0^2}{\omega},\quad \Gamma_0\equiv\frac{\Gamma k_0^3}{\rho\omega^2},\quad G_0\equiv\frac{gk_0}{\omega^2}, \tag{3}$$

where g is the usual gravitational acceleration, ω is the forcing frequency, ν is the kinematic viscosity, ρ is the density, and Γ is the surface tension. The wave number k_0 is chosen to satisfy the inviscid dispersion relation

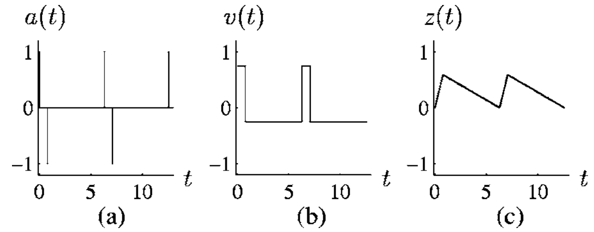

FIG. 1. Examples of (a) acceleration, (b) velocity, and (c) position of the fluid container over time in the case of two impulses per period. The positions of the vertical lines in the acceleration function denote the locations of the delta functions; here they have equal magnitude.

$$gk_0 + \frac{\Gamma k_0^3}{\rho} = \left(\frac{\omega}{2}\right)^2, \quad (4)$$

where $\omega/2$ is the frequency associated with the typical subharmonic response of Faraday waves. After dividing (4) by ω^2 we find $G_0+\Gamma_0=\frac{1}{4}$. $G(t)$ describes the applied acceleration; since time has been scaled by the forcing frequency ω, the dimensionless period of $G(t)$ is 2π.

We write the impulsive forcing function in the form

$$G_{imp}(t) = \sum_{n=-\infty}^{\infty} f_n \delta(t-t_n). \quad (5)$$

It is parametrized by the locations t_n of the impulses ($t_n < t_{n+1}, t_{n+N}-t_n=2\pi$) and by the amplitudes f_n ($f_{n+N}=f_n$), where N is the number of impulses in the repeating sequence. The dimensionless amplitude f_n of an impulse is given by

$$f_n \equiv \frac{v_n k_0}{\omega}, \quad (6)$$

where v_n is the jump in velocity at time t_n. We also require

$$\sum_{n=1}^{N} f_n = 0, \quad (7)$$

to prevent a net translation of the container. An example of an impulsive acceleration function, along with the corresponding velocity and position functions, is shown in Fig. 1.

B. Linear stability analysis

1. Calculations

Our linear stability calculations follow the method of [24]. From (1), the linear stability problem takes the form

$$((\partial_t - \gamma\nabla^2)^2 - \hat{D}\{\Gamma_0\nabla^2 - [G_0 - G(t)]\})h(x,t) = 0. \quad (8)$$

We then write $h(\mathbf{x},t)=p_k(t)e^{i\mathbf{k}\cdot\mathbf{x}}+$c.c., where c.c. denotes complex conjugate, and find that $p_k(t)$ satisfies

$$p_k'' + 2\gamma k^2 p_k' + \{\gamma^2 k^4 + \Gamma_0 k^3 + [G_0 - G(t)]k\}p_k = 0, \quad (9)$$

where the k subscript emphasizes the dependence of the solution on the perturbation wave number $k=|\mathbf{k}|$. Hereafter we focus on $k\neq 0$; the $k=0$ mode cannot be excited due to mass conservation.

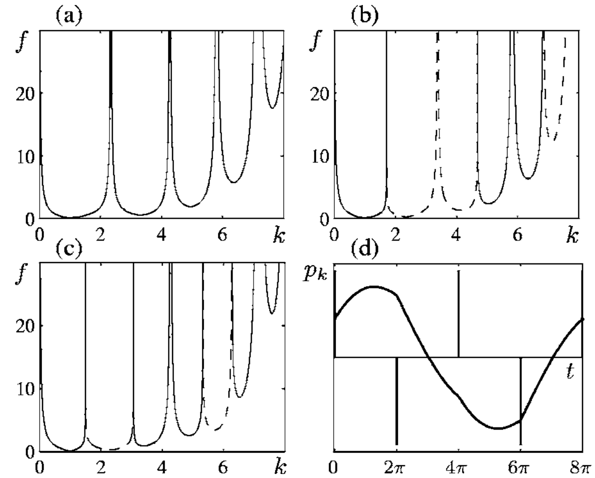

FIG. 2. (a)–(c) Examples of neutral stability curves $f(k)$ from (21) for various two-impulse forcing functions. Solid curves correspond to subharmonic tongues (Floquet multiplier −1), while dashed curves indicate harmonic tongues (Floquet multiplier +1). The spacing of the impulses in (18) is such that (a) $\Delta=0$, (b) $\Delta=\frac{1}{3}$, (c) $\Delta=\frac{1}{2}$. The dimensionless parameters in the calculations are $\gamma=0.02$ and $\Gamma_0=0.04$ (corresponding to fluid parameters $\nu=0.1$ cm^2/s, $\Gamma=16$ dyn/cm, $\rho=1$ g/cm^3, and $\omega/2\pi=20$ Hz). (d) Eigenfunction $p_k(t)$ at $k=k_c$, $f=f_c$ for an impulsive forcing function with equally-spaced impulses, indicated by vertical lines. The dimensionless parameters used are $\gamma=0.17$, $\Gamma_0=0.19$ (corresponding to physical parameters $\nu=0.20$ cm^2/s, $\Gamma=16$ dyn/cm, $\rho=1$ g/cm^3, and $\omega/2\pi=80$ Hz).

Between each impulse, (9) is simply the equation for a damped harmonic oscillator, with solution

$$p_k(t) = A_{k,n}e^{(-\gamma k^2 + i\omega_k)(t-t_n)} + \text{c.c.}, \quad t \in (t_n, t_{n+1}). \quad (10)$$

Here ω_k is the natural frequency of a wave with wave number k, which is determined by the dispersion relation

$$\omega_k^2 = \Gamma_0 k^3 + G_0 k. \quad (11)$$

We demand that $p_k(t)$ be continuous across each impulse, i.e., $p_k(t_n^+)=p_k(t_n^-)\equiv p_k(t_n)$, where $p_k(t_n^\pm)\equiv\lim_{t\to t_n^\pm}p_k(t)$. Integrating (9) across the nth impulse we obtain the following jump condition:

$$p_k'(t_n^+) - p_k'(t_n^-) = f_n k p_k(t_n). \quad (12)$$

This condition, together with the continuity requirement, yields the following map from $A_{k,n}$ to $A_{k,n+1}$:

$$\begin{pmatrix} A_{k,n+1}^r \\ A_{k,n+1}^i \end{pmatrix} = e^{-\gamma k^2 d_n} M_{k,n} \begin{pmatrix} A_{k,n}^r \\ A_{k,n}^i \end{pmatrix}, \quad (13)$$

where

$$M_{k,n} \equiv \begin{pmatrix} c_{k,n} & -s_{k,n} \\ s_{k,n} - F_{k,n+1}c_{k,n} & c_{k,n} + F_{k,n+1}s_{k,n} \end{pmatrix}. \quad (14)$$

Here $A_{k,n}^r$ ($A_{k,n}^i$) is the real (imaginary) part of $A_{k,n}$ and $c_{k,n}\equiv\cos(\omega_k d_n)$, $s_{k,n}\equiv\sin(\omega_k d_n)$, $F_{k,n}\equiv f_n k/\omega_k$. Note that

(14) depends on only two forcing parameters: $d_n \equiv t_{n+1} - t_n$, the time between the nth and $(n+1)$st impulses, and f_{n+1}, the strength of the $(n+1)$st impulse.

Piecing together the relationships between A_n and A_{n+1}, A_{n+1} and A_{n+2}, etc. across one period, we find the stroboscopic map that relates the solution of the linearized problem at time t_n to the solution one period later (i.e., after the sequence of N impulses):

$$\begin{pmatrix} A^r_{k,n+N} \\ A^i_{k,n+N} \end{pmatrix} = e^{-2\pi\gamma k^2} M_k \begin{pmatrix} A^r_{k,n} \\ A^i_{k,n} \end{pmatrix}. \tag{15}$$

Here $M_k \equiv M_{k,n+N-1} \cdots M_{k,n}$, where $M_{k,j}$ is given by (14).

The eigenvalues of $e^{-2\pi\gamma k^2} M_k$ determine the linear stability of the flat interface to disturbances of wave number k. Note that M_k has determinant one, so these eigenvalues $(\lambda_\pm)$ can be related to the trace of M_k by $e^{2\pi\gamma k^2}\lambda_\pm = \frac{1}{2}\mathrm{Tr}(M_k) \pm \sqrt{[\frac{1}{2}\mathrm{Tr}(M_k)]^2 - 1}$. An instability exists when both eigenvalues (Floquet multipliers) are real and the magnitude of one exceeds unity. The threshold condition is therefore

$$\frac{1}{2}\mathrm{Tr}(M_k) = \pm\cosh(2\pi\gamma k^2), \tag{16}$$

where "+" corresponds to the harmonic case (Floquet multiplier +1), and "−" corresponds to the subharmonic case (Floquet multiplier −1). This threshold condition defines an implicit equation $f(k)$ describing the neutral stability curves, where f is an appropriate measure of the overall impulse strength (e.g., for $N=2$ we use $f = |f_n| = |f_{n+1}|$).

Examples of neutral stability curves for various acceleration functions are presented in Figs. 2(a)–2(c) and 3. For values of f below the minimum of these curves, the trivial solution $(h = \Phi = 0)$ is stable. When f is increased above the critical forcing amplitude f_c at the curves' minimum (with corresponding critical wave number k_c), the flat surface solution becomes unstable to standing waves. An example of the associated critical eigenfunction, $p_k(t)$ $(k = k_c$ and $f = f_c)$, is shown in Fig. 2(d). Note the presence of kinks in $p_k(t)$ at the impulses, a consequence of the jump condition (12).

2. Linear stability results for N=2

We now focus our analysis on the case of two impulses per period by setting

$$f_n = (-1)^n f, \quad t_n = \pi\left(n + [1 - (-1)^n]\frac{\Delta}{2}\right) \tag{17}$$

in (5). Here

$$\Delta \equiv \frac{d_0 - d_1}{2\pi} \in (-1, 1) \tag{18}$$

measures the deviation from equal spacing of the impulses. Thus $\Delta = 0$ corresponds to equally-spaced impulses, and as $|\Delta|$ increases the spacing between the impulses becomes increasingly asymmetric; see Fig. 1 for an example where $\Delta < 0$.

It follows from (15) that $A_{k,n+2}$ and $A_{k,n}$ are related by

$$\begin{pmatrix} A^r_{k,n+2} \\ A^i_{k,n+2} \end{pmatrix} = e^{-2\pi\gamma k^2} \begin{pmatrix} \cos(2\pi\omega_k) - F_n c_n s_{n+1} & -\sin(2\pi\omega_k) + F_n s_n s_{n+1} \\ \sin(2\pi\omega_k) + F_n s_{n+1}(s_n + F_n c_n) & \cos(2\pi\omega_k) + F_n s_{n+1}(c_n - F_n s_n) \end{pmatrix} \begin{pmatrix} A^r_{k,n} \\ A^i_{k,n} \end{pmatrix}, \tag{19}$$

where

$$c_n \equiv \cos(\omega_k d_n), \quad s_n \equiv \sin(\omega_k d_n),$$

$$d_n = \pi[1 + (-1)^n \Delta], \quad F_n = \frac{f_n k}{\omega_k}. \tag{20}$$

Solving (16) for the neutral stability curves $f(k)$, we find

$$f(k) = \frac{2\omega_k}{k}\sqrt{\frac{\pm\cosh(2\pi\gamma k^2) - \cos(2\pi\omega_k)}{\cos(2\pi\omega_k) - \cos(2\pi\omega_k\Delta)}}, \tag{21}$$

where ω_k is given by (11). As before, "+" corresponds to the harmonic case and "−" to the subharmonic case. Note that $f(k)$ is invariant under $\Delta \to -\Delta$, so we can restrict to $\Delta \in [0, 1)$ for the remainder of the linear analysis. This is not, however, a symmetry of the full problem, and we will see that the sign of Δ affects the nonlinear response of the fluid to the impulsive forcing function.

We now examine in some detail the spacing and sequence of resonant tongues in the case of two impulses per period. For the purposes of this analysis, we use ω_k as the independent variable, where ω_k and k are related through the monotonic dispersion relation (11). We introduce

$$D(\omega_k) \equiv \cos(2\pi\omega_k) - \cos(2\pi\omega_k\Delta), \tag{22}$$

and denote the successive zeroes of $D(\omega_k)$ by ω_k^j $(\omega_k^j < \omega_k^{j+1}, \omega_k^0 = 0)$. The expression $f(k)$ for the neutral stability curves, given by (21), diverges at each ω_k^j, which leads to the structure of clearly demarcated resonance tongues seen in Figs. 2(a)–2(c). Since for $k > 0$ the numerator of the expression inside the square root in (21) is strictly positive in the harmonic case and negative in the subharmonic case, it follows that $D(\omega_k) > 0$ for harmonic resonance tongues and $D(\omega_k) < 0$ for subharmonic resonance tongues.

In the general case, resonance tongues will alternate between harmonic and subharmonic as k (equivalently, ω_k)

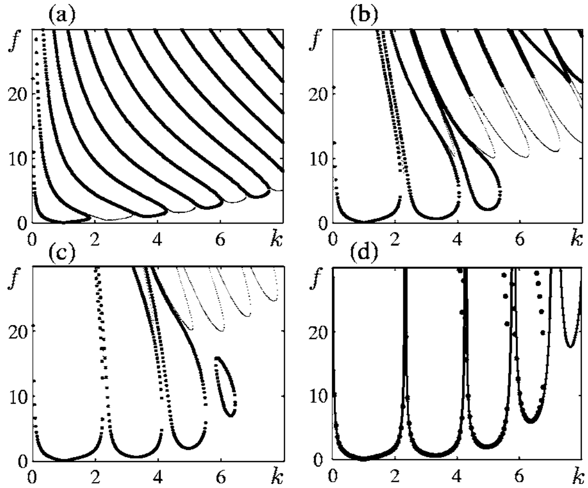

FIG. 3. Neutral stability curves for truncated Fourier series approximations of equally spaced impulses with (a) 1 term, (b) 10 terms, (c) 20 terms, and (d) 50 terms (with curves for equally-spaced impulses overlaid as solid lines). Large points correspond to subharmonic tongues and the smaller points to harmonic tongues. Parameters are the same as those in the neutral stability curves (a)–(c) of Fig. 2. Curves were generated using the method described in [18,22].

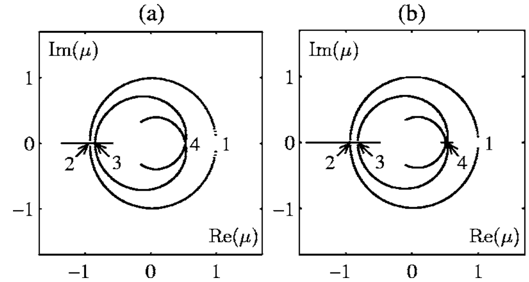

FIG. 4. Floquet multipliers $\mu_\pm$ associated with Eq. (19) plotted in the complex plane over the range $k \in [0,3]$ with $f = f_c(1+1.4)$ (this forcing is well above the onset value for the first resonance tongue but below onset for the second) for (a) equally-spaced impulses, and (b) sinusoidal forcing. These cases differ in that only for sinusoidal forcing do the Floquet multipliers split on the positive real axis. Fluid parameters are as in the neutral stability curves of Fig. 2(a)–2(c). Numbers indicate special points where $k=0$ (point 1), where complex Floquet multipliers meet on the negative real axis and split into two real values (point 2), where real Floquet multipliers recombine before splitting into a complex conjugate pair (point 3), and where complex Floquet multipliers meet on the positive real axis (point 4).

increases and $D(\omega_k)$ alternates in sign. However, for special values of Δ, successive subharmonic (or harmonic) tongues occur. Specifically, this happens for some j if $D(\omega_k^j) = D'(\omega_k^j) = 0$. We denote these double zeroes by $\hat{\omega}_k^m, m \in \mathbb{Z}^+$. It is straightforward to show that for $|\Delta| \neq 1$ these degenerate values occur only when $\cos(2\pi\hat{\omega}_k^m) = \cos(2\pi\hat{\omega}_k^m\Delta) = \pm 1$, which implies $\Delta = p/q$ for some coprime integers p, q $(0 \leqslant p < q)$. If p and q are both odd, then $\hat{\omega}_k^m = mq/2$; successive subharmonic (harmonic) tongues occur when m is even (odd). [See Fig. 2(b), generated with $\Delta = \frac{1}{3}$.] In contrast, if either p or q is even (or $p=0$), then only subharmonic tongues can occur in succession; when $\Delta \neq 0$ these are separated by vertical asymptotes at $\hat{\omega}_k^m = mq$ [see Fig. 2(a)], while when $\Delta = 0$ there are vertical asymptotes at each integer value of ω_k separating successive subharmonic tongues [see Fig. 2(c)]. In other words, there are no harmonic resonance tongues for equally-spaced impulses [Fig. 2(a)], as previously noted by Bechhoefer and Johnson [24].

3. Comparison with sinusoidal and multifrequency forcing

We now compare the linear stability results for equally-spaced impulsive forcing (i.e., $\Delta = 0$) with the corresponding results for sinusoidal forcing

$$G_{\sin}(t) = f_{\sin} \sin(t). \tag{23}$$

Here $f_{\sin} \equiv g_{\sin} k_0 / \omega^2$, where $g_{\sin}$ is the maximum (dimensioned) acceleration. [See Fig. 3(a) for an example of neutral stability curves in the case of sinusoidal forcing.] As noted earlier, the most striking difference between these two cases, manifest in the neutral stability curves (21), is the lack of harmonic tongues for the impulsive case. This difference is a consequence of the way that the Floquet multipliers associated with (19) move in the complex plane as the perturbation wave number k is varied, as illustrated in Fig. 4.

To further compare equally-spaced impulses and sinusoidal forcing, we consider the respective critical forcing strengths at the onset of standing waves, $f_{c,imp}$ and $f_{c,sin}$. In the limit of weak damping we may expand (21) about $\gamma = 0$ and $\omega_k = \frac{1}{2}$ (near the minimum of the neutral stability curves) to obtain

$$f_{c,imp} = \pi k_c \gamma [1 + O(\gamma^2)]. \tag{24}$$

For sinusoidal forcing and small damping we have

$$f_{c,sin} = 2 k_c \gamma [1 + O(\gamma^2)], \tag{25}$$

(see, for example, [31]). Thus $f_{c,imp}/f_{c,sin} = \pi/2 + O(\gamma^2)$. This is the same ratio that arises when considering (the first term in) the Fourier series expansion of the impulsive forcing function with $\Delta = 0$:

$$G_{imp}(t) = \frac{2}{\pi} f_{imp} \sum_{j=0}^{\infty} \cos[(2j+1)t]. \tag{26}$$

Here we have used (5) and (17) with $f_n = (-1)^n f_{imp}$. In Fig. 5(a) we plot the ratio $f_{c,imp}/f_{c,sin}$ as a function of forcing frequency (the most easily tuned parameter in experiments) for several viscosities. As anticipated, for small ν this ratio is well approximated by $\pi/2$. Furthermore, the ratio decreases with increasing viscosity (equivalently, γ) with a deviation $|1 - (2/\pi)(f_{c,imp}/f_{c,sin})| = O(\gamma^2)$.

We may also consider the effect of adding the next term, $\cos(3t)$, in the truncation of the Fourier series (26) and examine $f_{c,2}$, the critical value of this two-frequency forcing function, in the weak damping limit. [In general, $f_{c,M}$ denotes the dimensionless forcing strength at onset for the M-term truncation of (26).] It is demonstrated in [32] that for

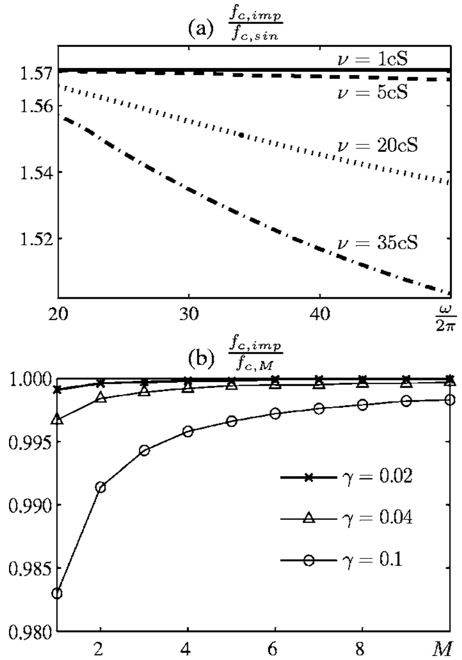

FIG. 5. (a) Ratio of critical forcing strength for impulsive and sinusoidal forcing as a function of forcing frequency (Hz). Viscosities are labeled in the figure; other parameters are as in the neutral stability curves (a)–(c) of Fig. 2. The solid line for $\nu=1cS$ is indistinguishable from a horizontal line at $\pi/2$. (b) Ratio of critical forcing strengths for equally-spaced impulses and the M-term truncated Fourier series, as a function of M, for $\Gamma_0=0.04$ and $\gamma=0.02$ (crosses), $\gamma=0.04$ (triangles), and $\gamma=0.1$ (open circles).

a two-frequency forcing function with commensurate frequencies $m\omega$ and $n\omega$ ($m\omega$ is assumed to drive the primary instability), the $n\omega$ frequency component is *destabilizing* when $m/n<\sqrt[4]{2}\approx 1.19$. By this we mean that the threshold for instability is lower in the two-frequency case than in the single frequency case. For the two-term truncation of (26), $m/n=\frac{1}{3}$ and hence we expect that $f_{c,2}<f_{c,1}=(\pi/2)f_{c,sin}$. Indeed, this is consistent with our finding that $f_{c,imp}/f_{c,sin}<\pi/2$ for impulsive forcing [see Fig. 5(a)].

As expected, adding more terms to the truncation of the Fourier series (26) results in a closer approximation to the critical forcing strength $f_{c,imp}$, as shown in Fig. 5(b). Despite this good agreement between $f_{c,imp}$ and $f_{c,M}$, the M-term truncated Fourier series is far less successful in capturing the behavior of the resonance tongues away from the minimum of the first tongue; this can be seen in Fig. 3. For $\gamma=0.02$ and $\Gamma_0=0.04$, for example, $f_{c,M}$ approximates $f_{c,imp}$ remarkably well even for small M [see the crosses in Fig. 5(b)]; however, with $M=50$, only the first four resonance tongues plausibly resemble those for impulsive forcing [see Fig. 3(d)].

III. WEAKLY NONLINEAR ANALYSIS

A. Weakly nonlinear calculation

We now extend our analysis of $N=2$ impulses to the weakly nonlinear regime in the case of one-dimensional waves. Following [33], we perform a multiscale expansion:

$$h(x,t,T)=\epsilon h_1(x,t,T)+\epsilon^2 h_2(x,t,T)+\cdots, \tag{27a}$$

$$\Phi(x,t,T)=\epsilon\Phi_1(x,t,T)+\epsilon^2\Phi_2(x,t,T)+\cdots, \tag{27b}$$

where $\epsilon\ll 1$, $T=\epsilon^2 t$ is a slow time, and the forcing amplitude is written $f=f_c(1+\epsilon^2 f_2)$. We seek spatially-periodic solutions in the separable Floquet-Fourier form:

$$h_1(x,t,T)=Z(T)p_1(t)e^{ik_cx}+\text{c.c.}, \tag{28a}$$

$$h_2(x,t,T)=Z^2(T)p_2(t)e^{2ik_cx}+\text{c.c.}, \tag{28b}$$

$$\Phi_1(x,t,T)=Z(T)q_1(t)e^{ik_cx}+\text{c.c.}, \tag{28c}$$

$$\Phi_2(x,t,T)=Z^2(T)q_2(t)e^{2ik_cx}+\text{c.c.}, \tag{28d}$$

where the critical wave number k_c, and the periodic eigenfunction $p_1(t)$ are determined from the linear stability analysis. Specifically, we take (k_c,f_c) to be the minimum of the neutral stability curves and use (10), evaluated at $k=k_c$ and with $|A_{k_c,n}|=1$, to obtain $p_1(t)$. The phase of $A_{k_c,n}$ is determined by the map (19), evaluated at $(k,f)=(k_c,f_c)$, and the (subharmonic) condition $p_1(t+2\pi)=-p_1(t)$ (equivalently, $A_{k_c,n+2}=-A_{k_c,n}$):

$$\frac{A^i_{k_c,n}}{A^r_{k_c,n}}=\frac{\cos(2\pi\omega_{k_c})-F_nc_ns_{n+1}+e^{2\pi\gamma k_c^2}}{-\sin(2\pi\omega_{k_c})+F_ns_ns_{n+1}}. \tag{29}$$

This expression defines the critical eigenmode associated with the instability. The subharmonic assumption $A_{k_c,n+2}=-A_{k_c,n}$ is valid when the instability is associated with the first resonance tongue, as it is for all parameters we have investigated. Plugging (28c) into (1a) yields $q_1(t)=(1/k_c)[p_1'(t)+\gamma k_c^2p_1(t)]$ at leading order in ϵ. Since in this section k will generally be fixed at its critical value, we hereafter drop this subscript from many expressions (e.g., we write A_n for $A_{k_c,n}$) or replace it with a subscript 1 [such as with $p_1(t)$].

At second order we find the equation [cf. (9)]

$$\begin{aligned}q_1^2={}&p_2''+2\gamma(2k_c)^2p_2'+\{\gamma^2(2k_c)^4+\Gamma_0(2k_c)^3\\&+[G_0-G(t)]2k_c\}p_2,\end{aligned} \tag{30}$$

which has the solution

$$\begin{aligned}p_2(t)={}&aA_n^2e^{2(-\gamma k_c^2+i\omega_1)(t-t_n)}+\frac{1}{2}b|A_n|^2e^{-2\gamma k_c^2(t-t_n)}\\&+B_ne^{(-\gamma(2k_c)^2+i\omega_2)(t-t_n)}+\text{c.c.},\end{aligned} \tag{31}$$

for $t\in(t_n,t_{n+1})$. Here

$$a=\frac{-2k_c\omega_1^2}{\omega_2^2-4\omega_1^2+4\gamma^2k_c^2+8i\gamma k^2\omega_1},$$

$$b = \frac{4k_c\omega_1^2}{\omega_2^2 + 4\gamma^2 k_c^4}, \tag{32}$$

and ω_1 (ω_2) is the natural frequency of a wave with wave number k_c $(2k_c)$ obtained from the dispersion relation (4). Note that the "homogeneous" solution to (30) must be included (i.e., $B_n \neq 0$) to ensure that $p_2(t)$ is continuous. Using this continuity condition and the jump condition on p_2' (obtained as in the linear stability calculation), we relate B_{n+1} to B_n through the map

$$\begin{pmatrix} B_{n+1}^r \\ B_{n+1}^i \end{pmatrix} = e^{-4\gamma k_c^2 d_n} M_{2,n} \begin{pmatrix} B_n^r \\ B_n^i \end{pmatrix} + R_n + bS_n. \tag{33}$$

Here $M_{2,n}$ is the matrix $M_{k,n}$ of (14) with $k=2k_c$; the vectors R_n and S_n are given in the Appendix. To obtain B_n, we require that $B_{n+2}=B_n$. [This harmonic condition is due to the fact that q_1^2, the driving term in (30), is 2π-periodic.]

At third order we obtain the solvability condition (see [33])

$$\tau \frac{dZ}{dT} = Lf_2 Z + (C_{res} + C_{non})|Z|^2 Z, \tag{34}$$

where τ, L, C_{res}, and C_{non} are given by

$$\tau = \frac{1}{2\pi}\int_{0^-}^{4\pi^-} (p_1' + \gamma k_c^2 p_1)\tilde{p}_1 dt = \frac{1}{2\pi}[A_0\tilde{A}_0(e^{i\omega_1 d_0} - 1) + A_1\tilde{A}_1(e^{i\omega_1 d_1} - 1) - 2i\omega_1(d_0\overline{A_0}\tilde{A}_0 + d_1\overline{A_1}\tilde{A}_1)] + \text{c.c.}, \tag{35a}$$

$$L = \frac{k_c}{4\pi}\int_{0^-}^{4\pi^-} \frac{G_{imp}(t)}{f} p_1\tilde{p}_1 dt = \frac{k_c}{2\pi}(A_0\tilde{A}_0 + A_0\bar{\tilde{A}}_0 - A_1\tilde{A}_1 - A_1\bar{\tilde{A}}_1) + \text{c.c.}, \tag{35b}$$

$$C_{res} = -\frac{k_c^2}{2\pi}\int_{0^-}^{4\pi^-} [(q_1p_2)' + \gamma k_c^2 q_1 p_2]\tilde{p}_1 dt, \tag{35c}$$

$$C_{non} = \frac{k_c^3}{4\pi}\int_{0^-}^{4\pi^-}\left[-(p_1^2 q_1)' - \gamma k_c^2 p_1^2 q_1 + k_c q_1^2 p_1 + \frac{3}{2}k_c^2\Gamma_0 p_1^3\right]\tilde{p}_1 dt. \tag{35d}$$

The full expressions for C_{res} and C_{non}, after integrating, are provided in the Appendix. In Eqs. (35) we use $\tilde{p}_1$ to denote the solution of the adjoint linear problem, which has the same form as (8) but with $\gamma \to -\gamma$. Hence

$$\tilde{p}_1(t) = \tilde{A}_n e^{(\gamma k^2 + i\omega_1)(t-t_n)} + \text{c.c.}, \quad t \in (t_n, t_{n+1}). \tag{36}$$

The map relating $\tilde{A}_{n+1}$ to $\tilde{A}_n$ is similarly obtained from (13) by replacing γ with $-\gamma$ and setting $k=k_c$. Note that in (34) we separate the cubic coefficient C into two distinct contributions, C_{res} (resonant) and C_{non} (nonresonant). The C_{res} term can be traced to quadratic nonlinearities in (1) (i.e., terms in which the k_c and $2k_c$ modes interact), while C_{non} derives from cubic nonlinearities and involves only the critical k_c mode.

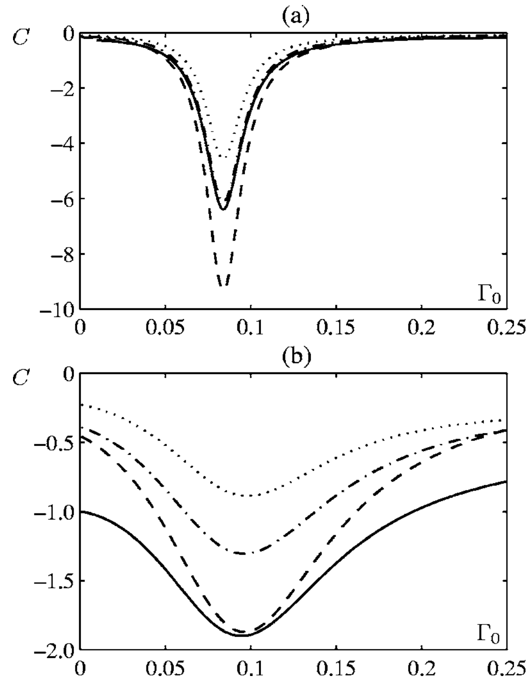

FIG. 6. Cubic coefficient in (34) as a function of Γ_0 with (a) $\gamma=0.01$ and (b) $\gamma=0.05$. The dashed line is the result for impulsive forcing with $\Delta=0.5$; the dot-dashed line is for $\Delta=0$; the dotted line is for $\Delta=-0.5$; the solid line is for sinusoidal forcing.

B. Weakly nonlinear results

We now examine in greater detail the cubic coefficient $C=C_{res}+C_{non}$, which determines the nonlinear saturation of the instability to standing waves. Figure 6 shows C as a function of the capillary parameter Γ_0 for various choices of Δ. We find, for most parameters, that $C(\Gamma_0)<0$, ensuring that the bifurcation to standing waves is supercritical. (We find subcritical bifurcations only in the capillary wave regime, $\Gamma_0 \approx 0.25$, and with extreme asymmetry, e.g., $\Delta \approx 0.99$.)

A dominant feature of the curves shown in Fig. 6 is the dip in C that reaches a minimum value at $\Gamma_0=\Gamma_{res}\approx 0.09$. This resonance feature is apparent both with impulsive forcing (nonsolid lines in Fig. 6) and with sinusoidal forcing (solid lines). For this figure we have used a normalization convention for $p_1(t)$ in the sinusoidal case which agrees with our normalization convention in the impulsive case ($|A_{k_c,n}|=1$) in the limit $\gamma \to 0$. Note that the sinusoidal and impulsive results agree quantitatively for $\gamma=0.01$ and $\Delta=0$. For larger damping ($\gamma=0.05$), the sinusoidal curve is shifted relative to the impulsive ones indicating a difference between their nonresonant contributions C_{non} to C.

In the sinusoidal case, the dip in C has been attributed to a 1:2 spatiotemporal resonance, i.e., at Γ_{res} we have $2\omega_1=\omega_2$ (see [23], for example). In particular, this feature, which scales with $1/\gamma$, is due to the strong coupling between the first subharmonic and the first harmonic modes, which are spatially commensurate at Γ_{res}. Since harmonic resonance tongues are entirely absent from the neutral stability picture for equally-spaced impulses, it is perhaps less apparent that an important (damped) harmonic mode can exist at $2k_c$. That there is such a damped harmonic mode (which, nonetheless, can never be excited) is evidenced by the appearance of the resonance dip in C at Γ_{res}. We can also determine directly the existence of a damped harmonic mode at $\Gamma \approx \Gamma_{res}$ by examining the Floquet multipliers associated with the linearized problem (19). We find that the Floquet multipliers cross the positive real axis as k is increased above k_c, which is the signature of a harmonic mode. Moreover, when $\Gamma = \Gamma_{res}$, the crossing occurs for $k = 2k_c$. See Fig. 4 for a comparison of the Floquet multipliers in the impulsive and sinusoidal cases.

A comparison of the (nonsolid) curves in Figs. 6(a) and 6(b) reveals that the spacing of the impulses can have a significant effect on the magnitude of the resonance feature. Some explanation for this behavior is suggested by recent results [29,30] on multifrequency-forced Faraday waves in which the form of the cubic amplitude equations is obtained from the spatial symmetries and the (weakly broken) symmetries of time translation, time reversal, and Hamiltonian structure. Here we are interested in the Fourier series expansion for an impulsive forcing function with two impulses per period:

$$G_{imp}(t) = \frac{f_{imp}}{2\pi} \sum_{j=1}^{\infty} (1 - e^{-ij[(1+\Delta)\pi]}) e^{ijt} + \text{c.c.} \tag{37}$$

In [29,30] the contribution of the damped $2k_c$ mode to the 1:2 spatiotemporal resonance is found to be most affected by the forcing frequency 2ω (where ω is the primary driving frequency) and its phase. This result suggests that we focus on the drastically truncated two-term Fourier series

$$G_2(t) = \frac{f_{imp}}{2\pi} [(1 + e^{-i\pi\Delta}) e^{it} + (1 - e^{-2i\pi\Delta}) e^{2it} + \text{c.c.}]. \tag{38}$$

At leading order in the damping γ, the onset of standing waves occurs when the magnitude of the first term in (38) becomes equal to γ (see, for example, [31]). Using

$$\frac{f_{imp}}{2\pi} |1 + e^{-i\pi\Delta}| = \gamma, \tag{39}$$

and simplifying the result through an appropriate time translation, we may rewrite (38) at onset as

$$G_2(t) = \gamma e^{it} + F_2 e^{2it} + \text{c.c.}, \tag{40}$$

where

$$F_2 = 2i\gamma \sin\left(\Delta \frac{\pi}{2}\right). \tag{41}$$

From Table 1 in [29] we find the predicted magnitude, at leading order in γ, of the resonant dip in the cubic coefficient at Γ_{res},

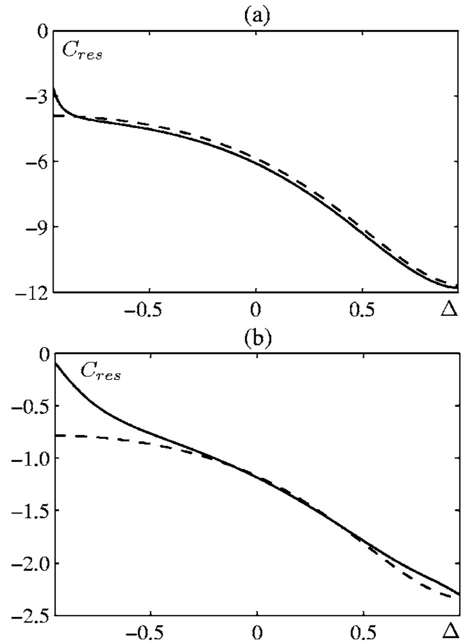

FIG. 7. Resonant contribution C_{res} to the cubic coefficient of Eq. (34) as a function of the asymmetry parameter Δ over the range $[-0.95, 0.95]$, calculated for the Zhang-Viñals equations using (A3) (solid line) and using multifrequency forcing results (43) with $\alpha_1 = 0.235$ (dashed line). Plots are for (a) $\gamma = 0.01$, and (b) $\gamma = 0.05$.

$$C_{res}^{2f} = -\alpha_1 \frac{|L_3| + \mu_i |f_{2\Omega}| \sin \Phi}{|L_3|^2 - |\mu_i f_{2\Omega}|^2}, \tag{42}$$

Here $|f_{2\Omega}| = |F_2| = 2\gamma |\sin(\Delta\pi/2)|$, $\Phi = \arg(F_2) = \text{sgn}(\Delta)\pi/2$, L_3 is the linear damping coefficient of the $2k_c$ mode $[L_3 = (2k_c)^2 \gamma \approx 4\gamma]$, and μ_i is the coefficient of the linear parametric driving term for the $2k_c$ mode ($\mu_i = 2k_c/2 \approx 1$). Thus C_{res}^{2f}, as a function of the asymmetry parameter Δ, becomes

$$C_{res}^{2f}(\Delta) \approx -\frac{\alpha_1}{2\gamma \left[2 - \sin\left(\frac{\Delta\pi}{2} \right) \right]}. \tag{43}$$

The constant α_1 is positive and must be determined by a nonlinear calculation; it depends on Γ_0, but not, at leading order, on γ. Here we choose α_1 such that the values of the multifrequency prediction $C_{res}^{2f}(\Delta)$ and our direct calculation of $C_{res}(\Delta)$ at $\Gamma_0 = \Gamma_{res}$ from (A3) agree for small damping ($\gamma = 0.001$) at $\Delta = 0$. (We then use the same estimate of α_1 throughout this comparison.) In Fig. 7, we compare $C_{res}(\Delta)$ with the multifrequency prediction and find good agreement, especially for small γ where the multifrequency results are expected to be valid. This agreement breaks down as $|\Delta|$ approaches unity (even more so for larger γ), an effect that is not overly surprising given that $|\Delta| \to 1$ is an unphysical limit requiring an infinite value of f_{imp} to produce standing waves [see (39)]. Note that C_{res}^{2f}, given by (43), scales with γ^{-1}, which explains the difference in scales evident in Figs. 6(a) and 6(b).

IV. DISCUSSION AND CONCLUSIONS

In this paper we examined the problem of Faraday waves parametrically excited by a periodic sequence of impulses (delta functions). We showed how to extend the linear stability analysis presented in [24] to include more general impulsive forcing functions, and investigated the weakly nonlinear regime for one-dimensional surface waves in the case of two impulses per period, comparing both linear and nonlinear results with the more established cases of sinusoidal and multifrequency forcing. Our analytical and numerical work was conducted within the framework of the Zhang-Viñals Faraday wave model, appropriate for describing small amplitude surface waves on deep, weakly-viscous fluid layers.

One theoretical advantage of using an idealized impulsive forcing function is that it allows for an exact, albeit generally implicit, expression for the neutral stability curves associated with the primary instability. Moreover, since the stroboscopic map characterizing the linear problem can be explicitly constructed, Floquet multipliers can be readily determined as a function of forcing and fluid parameters. This stands in sharp contrast to the sinusoidal and multifrequency cases where even the neutral curves must be determined numerically or through an asymptotic expansion that assumes weak damping and forcing. A further consequence of exactly solving the linear problem is that we are then able to derive explicit, analytic expressions for the amplitude of weakly nonlinear surface waves as a function of forcing and fluid parameters.

By varying the spacing between the up and down impulses making up the 2π-periodic forcing function for $N=2$, we found that the magnitude of the 1:2 resonance effect depends dramatically, and monotonically, on the corresponding asymmetry parameter Δ. Appealing to recent results on multifrequency forced Faraday waves [30], valid in the limit of weak damping, we obtained a prediction of this dependence based on a truncated two-term Fourier series approximation. This prediction agreed quite well with the results for impulsive forcing despite the severity of the approximation involved.

We envision several ways in which this work could be extended. For example, the methods used in this paper could be easily applied to the case of piecewise constant forcing, a type of driving function that has been explored in other systems (see [26,34], for instance) where it also led to analytic results. It would further be of interest to extend our weakly nonlinear analysis to the case of two-dimensional patterns. In such a context, additional questions of pattern selection, as well as more specific comparisons with multifrequency forcing, could be explored. One could try, for example, to construct impulsive forcing functions that mimic specific effects seen with multifrequency forcing. In this way the analytic results available for impulsive forcing would complement the numerical [19,22,32] and experimental results [8–13,15,16] reported with multifrequency forcing.

ACKNOWLEDGMENTS

We thank Yu Ding, Cristian Huepe, Chad Topaz, and Paul Umbanhowar for many helpful discussions. A.C. is grateful for support through NSF-IGERT Grant No. DGE-9987577. M.S. acknowledges support through NSF Grant No. DMS-0309667, and NASA Grant No. NAG3-2364. J.P. acknowledges support through EPSRC Grant No. GR/R52879/01.

APPENDIX A: ANALYTIC EXPRESSIONS

The vectors given in (33) are

$$R_n = \begin{pmatrix} \mathrm{Re}[a(A_n^2 e^{(-\gamma k_c^2 + i\omega_1)2d_n} - A_{n+1}^2)] \\ \dfrac{2}{\omega_2}\,\mathrm{Re}[a(A_n^2 e^{(-\gamma k_c^2+i\omega_1)2d_n}[(-1)^n k_c f_c - \gamma k_c^2 - i\omega_1] + A_{n+1}^2(\gamma k_c^2 + i\omega_1))] \end{pmatrix}, \tag{A1}$$

and

$$S_n = \begin{pmatrix} \dfrac{1}{2}(|A_n|^2 e^{-2\gamma k_c^2 d_n} - |A_{n+1}|^2) \\ \dfrac{1}{\omega_2}\{|A_n|^2 e^{-2\gamma k_c^2 d_n}[(-1)^n 2k_c f_c - \gamma k_c^2] + |A_{n+1}|^2 \gamma k_c^2\} \end{pmatrix}. \tag{A2}$$

The expressions for a and b in these vectors are given by (32), and ω_1 (ω_2) satisfies the dispersion relation (4) with wave number k_c ($2k_c$).

The full expressions for the components (C_{res} and C_{non}) of the cubic coefficient in the solvability condition (34) are

$$\begin{aligned} C_{res} = \frac{-2i\omega_1 k_c}{\pi}\sum_{j=0,1} & A_j B_j \tilde{A}_j \frac{\beta_1^+ - i\omega_1}{\beta_1^+}(e^{\beta_1^+ d_j} - 1) - \bar{A}_j B_j \tilde{\bar{A}}_j \frac{\beta_1^- + i\omega_1}{\beta_1^-}(e^{\beta_1^- d_j} - 1) + \left(A_j B_j \tilde{\bar{A}}_j \frac{\beta_2 + i\omega_1}{\beta_2} - \bar{A}_j B_j \tilde{A}_j \frac{\beta_2 - i\omega_1}{\beta_2}\right)(e^{\beta_2 d_j} - 1) \\ & + \left(a A_j^3 \tilde{\bar{A}}_j \frac{\beta_3 + i\omega_1}{\beta_3} + (b-a)|A_j|^2 A_j \tilde{A}_j \frac{\beta_3 - i\omega_1}{\beta_3}\right)(e^{\beta_3 d_j} - 1) + a A_j^3 \tilde{A}_j \frac{\beta_4 - i\omega_1}{\beta_4}(e^{\beta_4 d_j} - 1) + (b-a) \\ & \times |A_j|^2 A_j \tilde{\bar{A}}_j \frac{2\gamma k_c^2 - i\omega_1}{2\gamma k_c^2}(e^{-2\gamma k_c^2 d_j} - 1) + \text{c.c.}, \end{aligned} \tag{A3}$$

$$C_{non} = \frac{k_c^2}{4\pi} \sum_{j=0,1} A_j^3 \tilde{A}_j \frac{3\Gamma_0 k_c^3 - 2i\omega_1 \beta_3}{\beta_4}(e^{\beta_4 d_j} - 1) + A_j |A_j|^2 \tilde{A}_j \frac{9\Gamma_0 k_c^3 - 2i\omega_1 \beta_3}{\beta_3}(e^{\beta_3 d_j} - 1) + A_j^3 \tilde{\tilde{A}}_j \frac{3\Gamma_0 k_c^3 - 2i\omega_1 \beta_3}{\beta_3}(e^{\beta_3 d_j} - 1)$$
$$+ A_j |A_j|^2 \tilde{\tilde{A}}_j \frac{9\Gamma_0 k_c^3 - i\omega_1 \beta_3}{-2\gamma k_c^2}(e^{-2\gamma k_c^2 d_j} - 1) + \text{c.c.}, \tag{A4}$$

where

$$\beta_1^{\pm} = -4\gamma k_c^2 + i(\pm 2\omega_1 + \omega_2), \quad \beta_2 = -4\gamma k_c^2 + i\omega_2, \quad \beta_3 = -2\gamma k_c^2 + 2i\omega_1, \quad \beta_4 = -2\gamma k_c^2 + 4i\omega_1. \tag{A5}$$

[1] M. Faraday, Philos. Trans. R. Soc. London **121**, 319 (1831).
[2] J. Miles and D. Henderson, Annu. Rev. Fluid Mech. **22**, 143 (1990).
[3] H. W. Müller, R. Friedrich, and D. Papathanassiou, in *Evolution of Spontaneous Structures in Dissipative Continuous Systems*, edited by F. H. Busse and S. C. Muller, Lecture Notes in Physics (Springer, Berlin, 1998), pp. 231–265.
[4] B. Christiansen, P. Alstrom, and M. T. Levinsen, Phys. Rev. Lett. **68**, 2157 (1992).
[5] A. Kudrolli and J. P. Gollub, Physica D **97**, 133 (1996).
[6] D. Binks and W. van de Water, Phys. Rev. Lett. **78**, 4043 (1997).
[7] C. Wagner, H. W. Müller, and K. Knorr, Phys. Rev. E **62**, R33 (2000).
[8] W. S. Edwards and S. Fauve, J. Fluid Mech. **278**, 123 (1994).
[9] A. Kudrolli, B. Pier, and J. P. Gollub, Physica D **123**, 99 (1998).
[10] H. Arbell and J. Fineberg, Phys. Rev. Lett. **81**, 4384 (1998).
[11] W. S. Edwards and S. Fauve, Phys. Rev. E **47**, R788 (1993).
[12] H. Arbell and J. Fineberg, Phys. Rev. Lett. **84**, 654 (2000).
[13] H. W. Müller, Phys. Rev. Lett. **71**, 3287 (1993).
[14] H. Arbell and J. Fineberg, Phys. Rev. Lett. **85**, 756 (2000).
[15] H. Arbell and J. Fineberg, Phys. Rev. E **65**, 036224 (2002).
[16] T. Epstein and J. Fineberg, Phys. Rev. Lett. **92**, 244502 (2004).
[17] T. B. Benjamin and F. Ursell, Proc. R. Soc. London, Ser. A **225**, 505 (1954).
[18] K. Kumar and L. S. Tuckerman, J. Fluid Mech. **279**, 49 (1994).
[19] J. Beyer and R. Friedrich, Phys. Rev. E **51**, 1162 (1995).
[20] K. Kumar, Proc. R. Soc. London, Ser. A **452**, 1113 (1996).
[21] P. Chen and J. Viñals, Phys. Rev. Lett. **79**, 2670 (1997).
[22] T. Besson, W. S. Edwards, and L. S. Tuckerman, Phys. Rev. E **54**, 507 (1996).
[23] W. Zhang and J. Viñals, J. Fluid Mech. **336**, 301 (1997).
[24] J. Bechhoefer and B. Johnson, Am. J. Phys. **64**, 1482 (1996).
[25] C. S. Hsu, J. Appl. Mech.-T. ASME 39, 551 (1972).
[26] C. S. Hsu and W. H. Cheng, J. Appl. Mech.-T. ASME E40, 78 (1973).
[27] V. N. Pilipchuk, S. A. Volkova, and G. A. Starushenko, J. Sound Vib. **222**, 307 (1999).
[28] C. Huepe and M. Silber (unpublished).
[29] J. Porter, C. M. Topaz, and M. Silber, Phys. Rev. Lett. **93**, 034502 (2004).
[30] C. M. Topaz, J. Porter, and M. Silber, Phys. Rev. E **70**, 066206 (2004).
[31] J. Porter and M. Silber, Physica D **190**, 93 (2004).
[32] C. M. Topaz and M. Silber, Physica D **172**, 1 (2002).
[33] M. Silber and A. C. Skeldon, Phys. Rev. E **59**, 5446 (1999).
[34] E. D. Yorke, Am. J. Phys. **46**, 285 (1978).